SCIENTIFIC REPORTS

OPEN

Iso-Oriented Anatase TiO_2 Mesocages as a High Performance Anode Material for Sodium-Ion Storage

Received: 19 March 2015
Accepted: 09 June 2015
Published: 06 July 2015

Zhensheng Hong[1], Kaiqiang Zhou[1], Zhigao Huang[1] & Mingdeng Wei[2,3]

A major obstacle in realizing Na-ion batteries (NIBs) is the absence of suitable anode materials. Herein, we firstly report the anatase TiO_2 mesocages constructed by crystallographically oriented nanoparticle subunits as a high performance anode for NIBs. The mesocages with tunable microstructures, high surface area (204 m^2 g^{-1}) and uniform mesoporous structure were firstly prepared by a general synthesis method under the assist of sodium dodecyl sulfate (SDS). It's notable that the TiO_2 mesocages exhibit a large reversible capacity and good rate capability. A stable capacity of 93 mAhg^{-1} can be retained after 500 cycles at 10C in the range of 0.01–2.5V, indicating high rate performance and good cycling stability. This could be due to the uniform architecture of iso-oriented mesocage structure with few grain boundaries and nanoporous nature, allowing fast electron and ion transport, and providing more active sites as well as freedom for volume change during Na-ion insertion. CV measurements demonstrate that the sodium-ion storage process of anatase mesocages is mainly controlled by pseudocapacitive behavior, which is different from the lithium-ion storage and further facilitates the high rate capability.

Developing the rechargeable batteries is critical to address the increasing demand of mobile devices, electric-powered transportation, and stationary energy storage. Lithium-ion batteries (LIBs) have been the most promising battery technology owing to their higher energy density and longer cycle life than other secondary battery systems[1]. However, there is increasing concern about the cost and the limitation of lithium reserves on earth for large-scale applications of LIBs[2]. Sodium is a cheap, abundant and second lightest alkali metal element, and thus has recently attracted great interest for the use as a transporting ion for alternative rechargeable batteries[3–5]. However, the larger diameter of the Na-ion (0.97 Å) compared to Li-ion (0.68 Å) hampers electrochemical reaction kinetics, which makes it difficult to find suitable host materials which have sufficiently large interstitial space to accommodate sodium ions and can allow reversible and rapid ion/electron insertion and extraction[6].

Now, a major obstacle in realizing Na-ion batteries (NIBs) was the absence of suitable negative electrodes[4]. Graphite was found to be good host material for Li intercalation, and is now commercially utilized as negative electrode materials for LIBs. In the previous study, graphite cannot be utilized as an insertion host of Na ions[6,7]. Recently, it has been shown that graphite can be used for sodium-ion batteries by making use of co-intercalation phenomena in spite of the poor rate performance[8]. Some studies of hard carbons as negative materials for NIBs were reported, however, it delivered limited capacity at high current rate[9,10]. Recently, some anode materials with alloy-type (Sn and SnO_2)[11,12] and conversion-type

[1]Fujian Provincial Key Laboratory of Quantum Manipulation and New Energy Materials, College of Physics and Energy, Fujian Normal University, Fuzhou, Fujian 350108, China. [2]State Key Laboratory of Photocatalysis on Energy and Environment, Fuzhou University, Fuzhou, Fujian 350002, China. [3]Institute of Advanced Energy Materials, Fuzhou University, Fuzhou, Fujian 350002, China. Correspondence and requests for materials should be addressed to Z.H. (email: wintero514@163.com) or M.D.W. (email: wei-mingdeng@fzu.edu.cn)

mechanism (CuO and MoS_2)[13,14] were studied, which showed high initial capacity but suffered from poor cycling performance owing to the large volume change or the sluggish kinetics. Classical insertion materials such as $Na_2Ti_3O_7$ was proposed as an alternative anode material operating at a low potential of around 0.3 V vs. Na/Na^+, however, such a material showed a rather low capacity and poor cycling stability[15,16]. Therefore, it is still a challenge to develop appropriate anode materials with both high capacity and long cycling life.

Several types of TiO_2 polymorphs have been used as promising anode materials for LIBs due to its intrinsic advantages in safety, low cost and good cyclic stability[17–20]. However, only few reports were reported so far on the behavior of Na ions insertion into TiO_2. Although Rajh *et al.*[21] firstly investigated the amorphous TiO_2 nanotube anode for rechargeable NIBs, they concluded that anatase TiO_2 is inactive in their NIBs. Most recently, it's found that the Na-ion storage performance of anatase TiO_2 nanostructures could be improved by carbon coating or graphene doping[22–25]. However, there are different opinions about the sodium storage process. Cha *et al.*[24] and Kim *et al.*[25] claimed the similar suggestion that sodium ions would be reversibly (de-)inserted into the anatase host observed from the lattice expansion and structure remaining during the intercalation and extraction process. On the contrary, Wu *et al.*[26] very recently reported that the anatase TiO_2 would be partly reduced to metallic titanium and amorphous sodium titanate phase which could reversibly store about 0.41 sodium per TiO_2. These results encourage further study on developing an ideal nanostructure of this new promising anode material for NIBs and exploring their Na-ion storage mechanism.

Herein, we describe a general and facile synthesis route of iso-oriented TiO_2 mesocages with tunable microstructures and nanoporous nature and their application as high-performance anode in rechargeable Na-ion batteries. It's notable that the obtained TiO_2 mesocages are built by very tiny nanocrystals with a mutual orientation, holding a fine nanoporous structure and large surface area. The obtained iso-oriented TiO_2 mesocages exhibited large capacity and good cycling stability for NIBs. The sodium ions storage is mainly controlled by the pseudocapacitive process, which facilitates the high-rate capability.

Results

The iso-oriented TiO_2 mesocages were synthesized by a simple and low-temperature route. The samples obtained from HNO_3 and HCl solution were defined as TiO_2-MN and TiO_2-MC, respectivley. Figure 1a shows the related X-ray diffraction (XRD) patterns of as-prepared samples. All the diffraction peaks in Fig. 1 could be exclusively ascribed to tetragonal anatase TiO_2 (JCPDS 73-1764). The broadened diffraction peaks suggest a small crystallite size of the anatase samples. The average crystallite size of TiO_2-MN was calculated to be approximately 11 nm (also 11 nm for TiO_2 -MC), using the Scherer equation, based on the (101) diffraction peak. N_2 adsorption–desorption isotherms measurements were adopted to reveal the Brunauer–Emmett–Teller (BET) surface area and pore size distribution, as shown in Fig. 1b,c. The BET surface area and the pore volume of TiO_2-MN were determined to be 204 $m^2\ g^{-1}$ and 0.62 $cm^3\ g^{-1}$, respectively. Morover, TiO_2-MN exhibits rather uniform nanopores with an average diameter of 5.0 nm in Fig. 1b (inset). Compared to TiO_2-MC (Fig. 1c), its BET surface area and pore volume were about 199 $m^2\ g^{-1}$ and 0.31 $cm^3\ g^{-1}$, suggesting a lower pore volume and a smaller pore size mostly around 2.7 nm.

Figure 2a,b show the low-magnification and high-magnification SEM image of the sample obtained from 2 M HNO_3 aqueous solution (TiO_2-MN), indicating the large-scale formation of nanoparticles with a size of about 30–50 nm. The rough surface and porous nature of the nanoparticles could also be clearly observed (Fig. 2b). The TEM image shown in Fig. 2c further reveals the porous structure of TiO_2-MN. Figure 2d presents a typical TEM image of a single nanoparticle, which confirms that the anatase TiO_2 nanoparticle was constructed from tiny nanoparticle subunits with diameter about 5 nm and has a cage-like morphology with nanoporous structure. As shown in the upper inset of Fig. 2d, the SAED pattern taken from the whole nanoparticle exhibited single-crystal-like diffraction, suggesting that the tiny nanoparticle subunits were highly ordered and oriented along the [100] direction. The HRTEM image (inset of Fig. 2d) further confirms that the primary nanocrystals were highly crystalline, the clear lattice fringe of 0.19 nm was assigned to the (200) spacing of anatase structure. It should be pointed that similar single-crystal-like TiO_2 mesocages were synthesized by Lu *et al.*[27] through a hard-template (SBA-15) method and demonstrated excellent photocatalytic activity. Herein, the iso-oriented TiO_2 mesocages with high surface area and uniform mesopores, constructed by highly oriented tiny nanocrystals, were successfully prepared by a facile and low-temperature route.

It's notable that the iso-oriented TiO_2 mesocages with tunable microstructures could be prepared by using different anion in this synthesis method. SEM and TEM images of TiO_2-MC obtained from 2 M HCl aqueous solution are shown in Fig. 3. It is clearly shown that numerous nanoparticles with uniform size (40–60 nm) were formed. TiO_2-MN possessed of a rough surface, actually, it was constructed by tiny nanoparticle subunits (about 3–5 nm). The corresponding SAED pattern in the inset of Fig. 3d for the whole nanoparticle with single-crystal-like diffractions indicates that the building of nanoparticle subunits were highly ordered, leading to the formation of a crystallographically oriented architecture along [001] direction. Such architecture was named mesocrystal by Cölfen *et al.* which is porous quasi-single crystal consisting of ordered assemblies of aligned nanoparticles [28]. Furthermore, the diffraction spots were slightly elongated (similar results were observed for TiO_2-MN), indicating that there was a small mismatch between the boundaries of the nanoparticle subunits; this is usually found for the growth

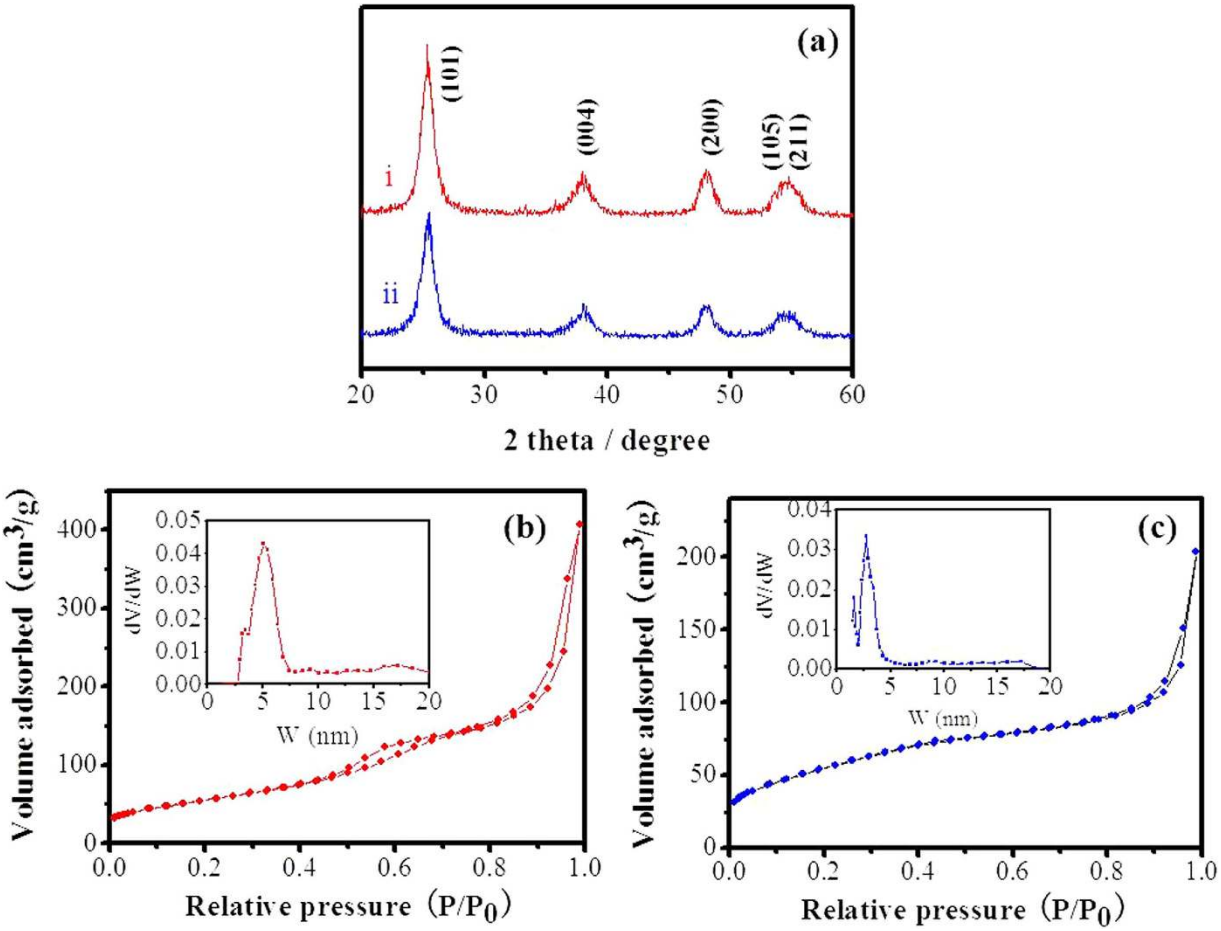

Figure 1. (**a**) XRD patterns of TiO_2-MN (curve i) and TiO_2-MC (curve ii), N_2 adsorption-desorption isotherms of (**b**) TiO_2-MN and TiO_2-MC. The insets in (**b**) and (**c**) are the corresponding NLDFT pore size distribution.

of many ordered nanoparticle assembles (mesocrystals) when they are assembled in the same orientation[28,29].

To shed light on the formation mechanism of the TiO_2 mesocages, a series of samples were synthesized for different periods of time and the results are shown in Figure S1. It could be observed that some irregular particles were constructed by the tiny anatase TiO_2 nanocrystals, the boundaries among the nanocrystals were clear and they aggregated together by perfect or imperfect attachments. It's demonstrated that aggregation of nanocrystals with the same crystallographic orientations, as well as the presence of defects, are strong evidence of oriented attachment (OA)[30,31]. This growth mechanism is also a typical formation process for the ordered nanoparticle superstructures (mesocrystals)[28]. Besides the anion (NO_3^- and Cl^-), the amount of the SDS significantly affect the morphology of the final samples, more SEM images were shown in Figure S2. Therefore, the microstructures of the obtained TiO_2 mesocages depend on the cooperative effect of the surfactant and anion. It was pointed out that the organic additive could be in favor of the temporary stabilization of the primary nanocrystals, allowing their attachment and assembly into ordered aggregates[28,29]. The driving force for the oriented self-assembly could be assigned to the minimization of the total surface energy of disordered primary nanocrystals[28].

Finally, the sodium-ion storage properties of the iso-oriented TiO_2 mesocages with mesoporous structure were investigated. Cells made from commercial anatase TiO_2 nanoparticles (TiO_2-NPs) were also fabricated as a reference sample. The XRD, SEM image and N_2 adsorption-desorption isotherms of TiO_2-NPs were shown in Figure S3. The BET surface area and the pore volume of TiO_2-NPs were determined to be 118 $m^2\ g^{-1}$ and 0.32 $cm^3\ g^{-1}$, respectively. Figure 4a shows the rate capability of TiO_2-MN, TiO_2-MC and TiO_2-NPs from 0.2 to 5 C (1C = 170 mAg^{-1}). TiO_2-MN exhibited good rate performance, with a stable capacity of 240 $mAhg^{-1}$ at 0.5 C, 200 $mAhg^{-1}$ at 1 C, 165 $mAhg^{-1}$ at 2 C, and 137 $mAhg^{-1}$ at 5 C, 120 $mAhg^{-1}$ at 10 C. Furthermore, a reversible capacity of 180 $mAhg^{-1}$ could be remained when the current rate returned to 1 C. TiO_2-MC showed comparable performance at low current rates, but was not so good as TiO_2-MN at high current rates which may be due to the lower pore volume and smaller pore

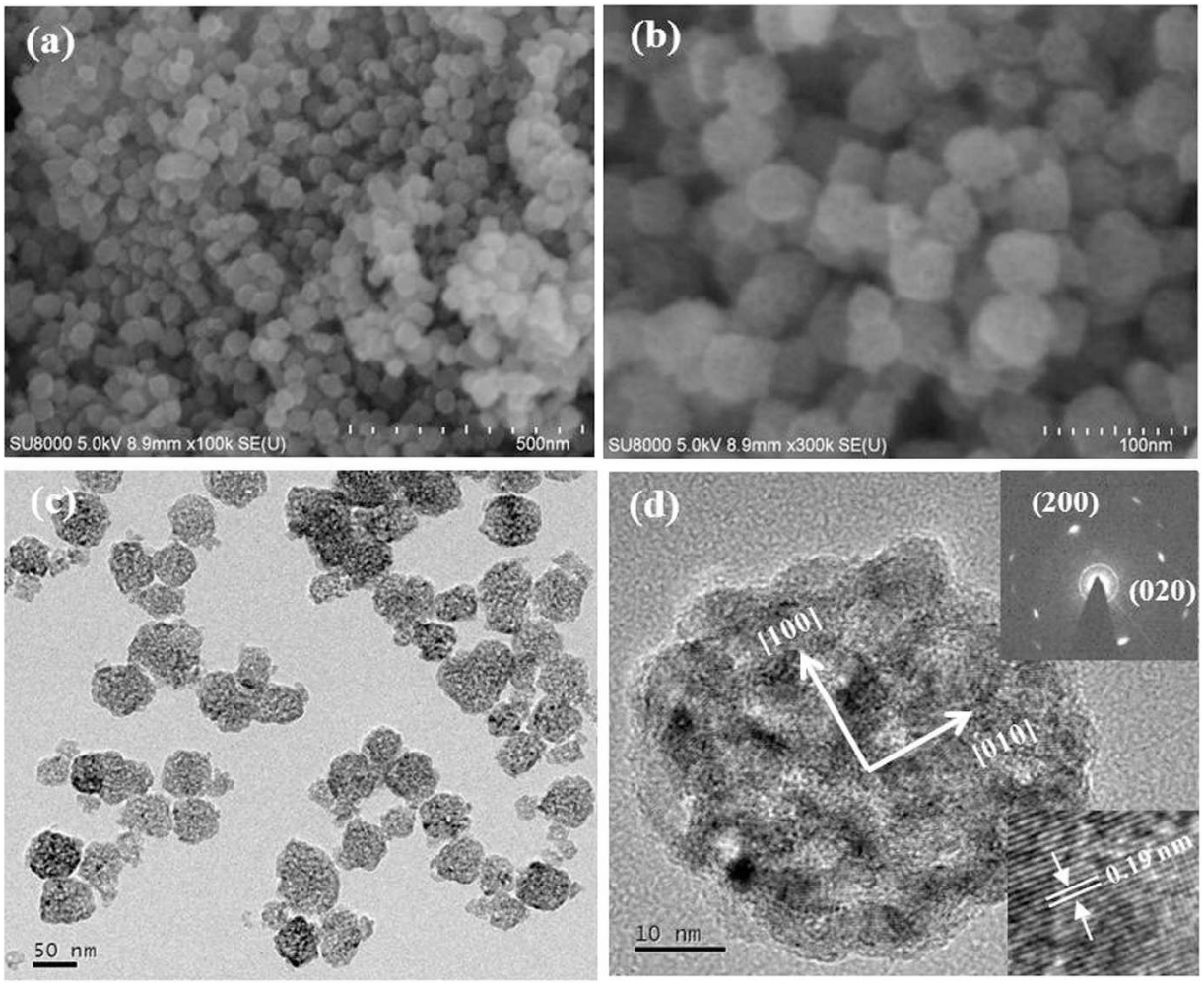

Figure 2. SEM (**a**, **b**) and TEM (**c**, **d**) images of TiO_2-MN. The insets in (**d**) are the related SAED pattern and HRTEM image, respectively.

size. However, both TiO_2-MN and TiO_2-MC exhibited superior rate performance compared to TiO_2 nanoparticles. It displays a stable discharge capacity of 160 $mAhg^{-1}$ at 0.5 C, 125 $mAhg^{-1}$ at 1 C, 97 $mAhg^{-1}$ at 2 C, and 64 $mAhg^{-1}$ at 5 C, 38 $mAhg^{-1}$ at 10 C. Figure 4b shows typical charge-discharge profiles of the three samples at the second cycle, the slope profiles are similar to the previous reports of anatase TiO_2 as anode material for Na-ion batteries[22–25]. The character of the charge-discharge profiles was not apparently changed during cycling (Fig. 4c). Figure 4d presents the cycling performance of TiO_2-MN and TiO_2-MC, the capacity of 152 $mAhg^{-1}$ and 128 $mAhg^{-1}$ could be remained, respectively, after 60 cycles at 1 C. In order to test the long cyclic stability at high rates, a sodium-ion cell made from TiO_2-MN were run at 10 C for 500 cycles, after aging at 0.5 C for 5 cycles. Figure 4e shows the capacity starts at 123 $mAhg^{-1}$ and still maintains at 93 $mAhg^{-1}$ after 500 cycles as well as high columbic efficiency, indicating a good cycling ability. Thus, anatase TiO_2 mesocages exhibit a larger capacity and better rate performance than that of layerd titanante nanotubes and nanorods[32,33]. It is suggested that (as the scheme in Fig. 4f) the crystallographically oriented anatase mesocages (composed of tiny nanocrystal subunits) were well connected with few grain boundaries compared with the irregularly oriented nanoparticles, which facilitated the fast Na^+ ion and electron transport. Moreover, the very large surface area and nanoporous nature in the mesocages could provide a high level of accessibility for the electrolyte and more active sites, and hence allow the efficient ion transport as well as the freedom for volume change.

Cyclic voltammetry (CV) experiments performed at various sweep rates (0.1–1 mV/s) were used to examine the redox processes occurring in the as-prepared iso-oriented TiO_2 mesocages. As shown in Fig. 5a, a couple of redox peaks are observed between 0.4 V and 0.9 V vs. Na/Na^+, which could correspond to the insertion/extraction of Na-ion. The voltammetric response of electrode active material with respect to sweep rate can be calculated according to[34]:

$$i = av^b$$

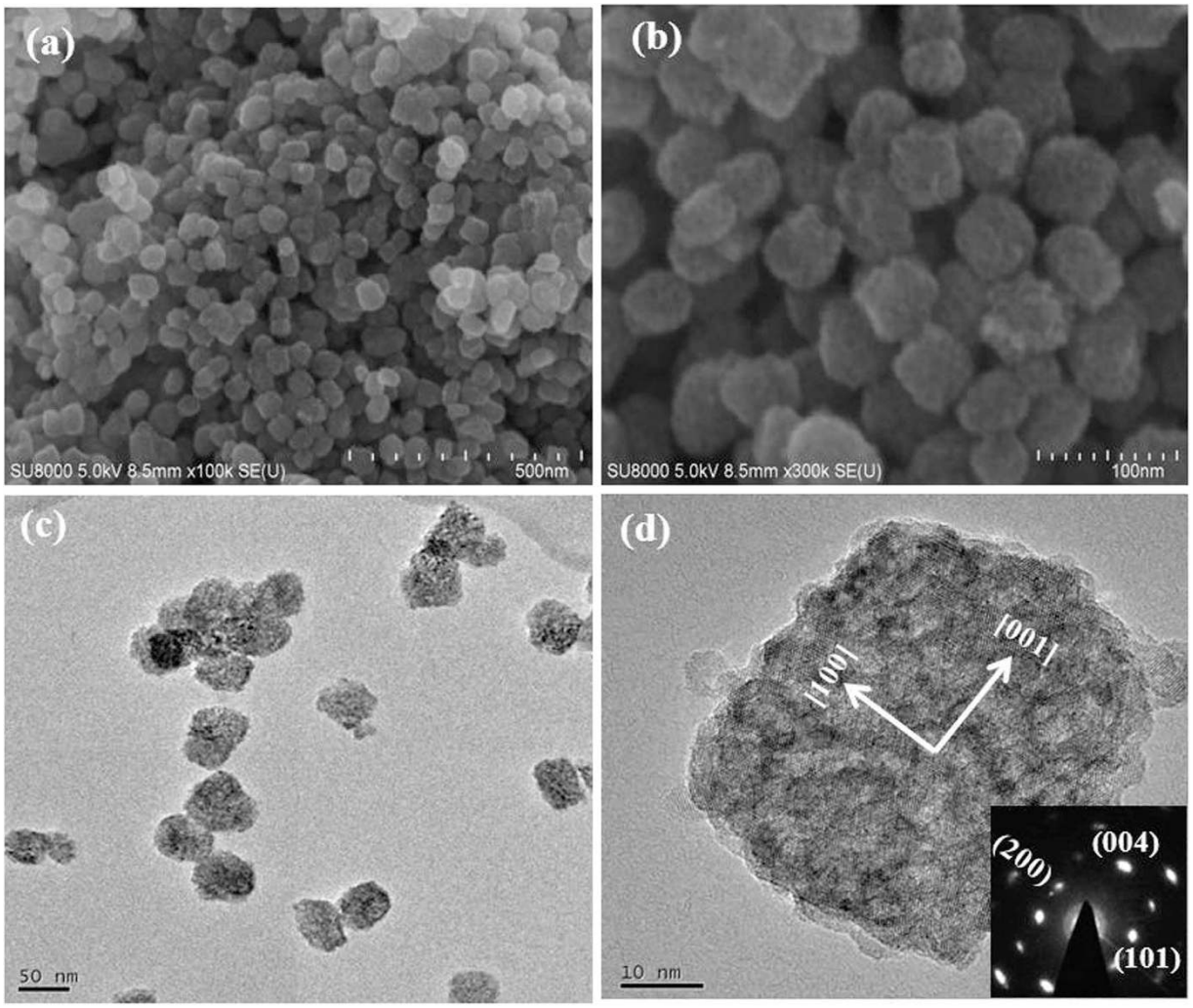

Figure 3. SEM (**a**, **b**) and TEM (**c**, **d**) images of TiO_2-MC. The inset in (**d**) is the related SAED pattern from the whole nanoparticle.

where *i* is the current density, *v* is the scan rate, and a and b are adjustable parameters. When the b-value approaches 1, the electrochemical process is mainly controlled by capacitance, and when the b value is close to 0.5, the insertion behavior (battery behavior) dominates. The pseudocapacitive behavior of electrode material arises from the surface faradic redox reactions, and the insertion behavior is controlled by bulk diffusion process. However, both of them displays obvious redox peaks on CV measurements in a specific voltage region. Figure 5b shows the relationship between peak current and sweep rate on NIBs. As the b-value approaches 1 (0.89 calculated from Fig. 5b), the sodium-ion storage of TiO_2 mesocages is mainly controlled by the pseudocapacitive process, leading to a fast Na^+ insertion/extraction and extended cycling life. Rajh *et al.*[21] also found the pseudocapacitive characteristic of the amorphous TiO_2 nanotube anode for rechargeable NIBs. However, the lithium-ion storage of the amorphous TiO_2 nanotube anode is controlled by capacitive process as the discharge voltage was below 1.8 V. In this study, a couple of typical redox peaks are observed from Fig. 5c, corresponding to the insertion/extraction of Li-ion. The b-value approaches 0.5 (0.58 calculated from Fig. 5d), demonstrating the typical insertion behavior of lithium storage in TiO_2 mesocages. Thus, the Na^+ and Li^+ ion storage performance of TiO_2 mesocages is mainly controlled by pseudocapacitive behavior and insertion behavior, respectively.

Recently, it's reported that anatase TiO_2 nanocrystals displayed a large irreversible capacity at the first cycle especially when the discharge voltage was below 0.3 V[35,26]. This large irreversible capacity could be due to occurrence of side reactions with electrolyte, a solid−electrolyte interface (SEI) formation and some irreversible electrochemical reaction of the active materials[25,26,35]. This phenomenon was also found in the $Na_2Ti_3O_7$ anode material for sodium-ion batteries[15,16]. Similar results were also found in this study, as shown in Fig. 6a. The TiO_2 nanoparticles (TiO_2-NPs) exhibited a discharge capacity of 436.3 $mAhg^{-1}$ and charge capacity of 163.5 $mAhg^{-1}$ at 0.5 C at the first cycle, indicating a low columbic efficiency of 37.4%. Besides, a large irreversible capacity of about 284 $mAhg^{-1}$ was observed under 0.3 V. However, TiO_2 mesocages displayed a large discharge and charge capacity of 586 $mAhg^{-1}$ and 270 $mAhg^{-1}$, and

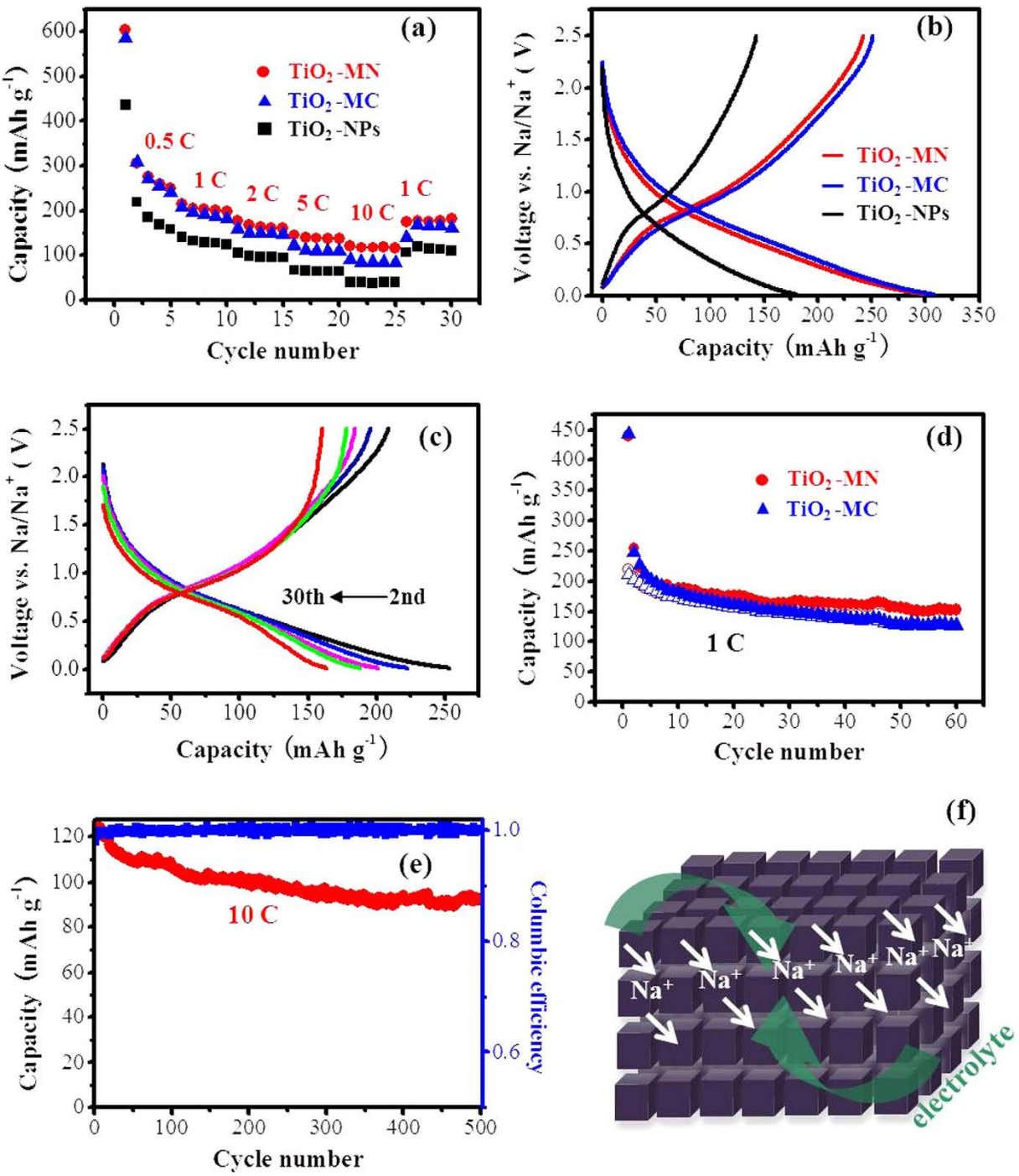

Figure 4. (**a**) Rate capability of TiO_2-MN, TiO_2-MC and TiO_2 nanoparticles from 0.2 to 5 C, (**b**) charge-discharge profiles of the three samples at a current rate of 0.5 C, (**c**) charge-discharge profiles of TiO_2-MN, (**d**) cycling performance of TiO_2-MN and TiO_2-MC (filled symbols: discharge capacity and open symbols: charge capacity), (**e**) long cycling performance of TiO_2-MN, (**f**) schemes of the electrochemical reaction process of TiO_2 mesocages.

thus higher columbic efficiency of 46.1%. Moreover, the irreversible capacity (180 $mAhg^{-1}$) under 0.3 V is also smaller than that of TiO_2-NPs. This could be due to the crystallographically oriented mesocages with few grain boundaries compared with the irregularly oriented nanoparticles, leading to less irreversible reaction and fast electron transport.

It's well known that Raman spectroscopy is an effective measurement to investigate the structure of titanium dioxide, and the results are shown in Fig. 6b. The curve of fresh electrode exhibits the typical

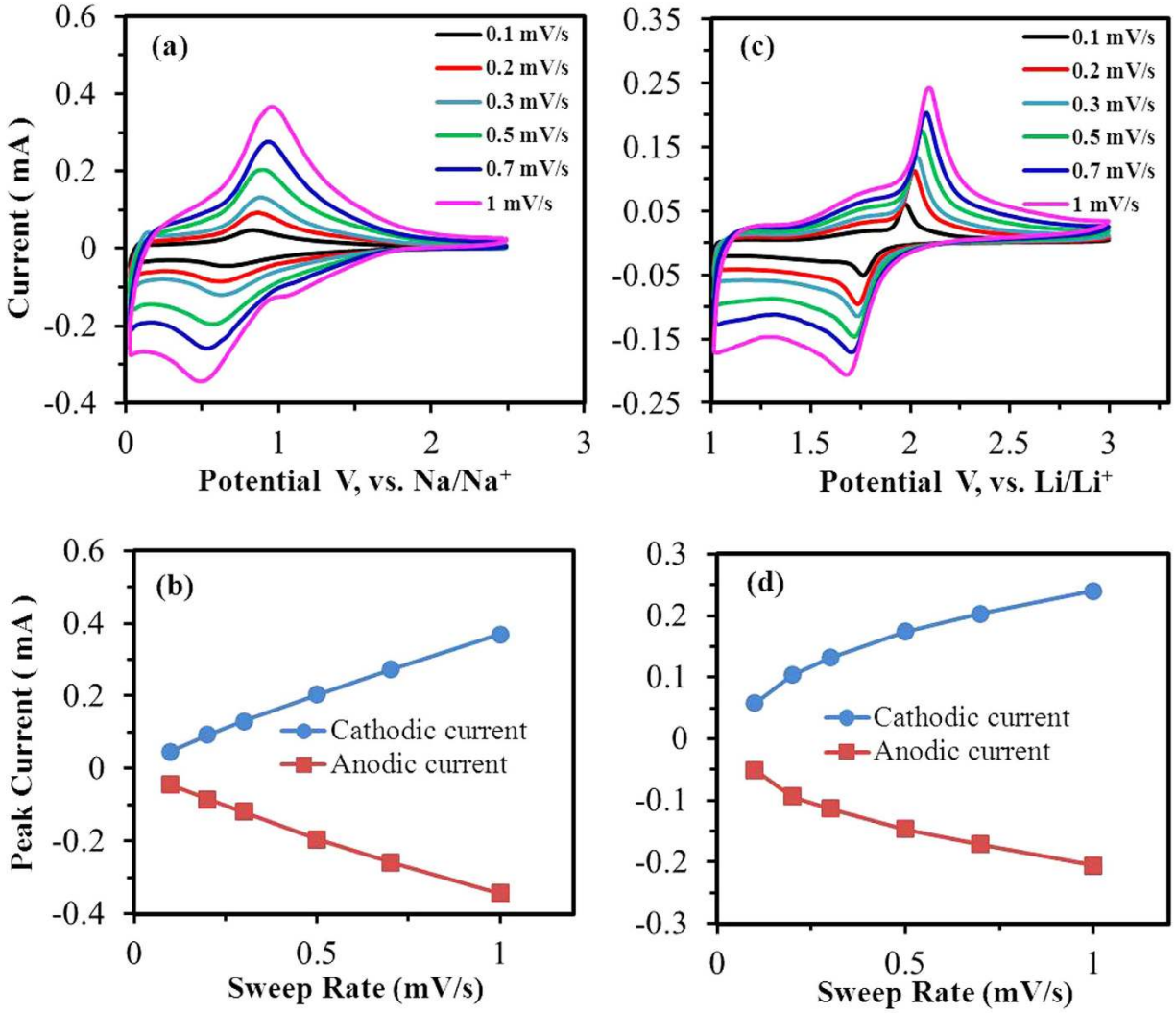

Figure 5. Cyclic voltammetry curves at various sweep rates (**a**, **c**) and the relationship between peak current and sweep rate of TiO_2-MC (**b**, **d**): (**a**, **b**) sodium-ion battery, (**c**, **d**) lithium-ion battery.

Raman peaks of anatase TiO_2[36]. During the discharge and charge process, the Raman spectra of the electrode suggest that the crystallinity of the anatase TiO_2 continuously weakens, which is in agreement with the results reported by Wu *et al.*[26] However, the morphology of the TiO_2 mesocages remarkably remained unchanged even after different rate cycling, as displayed in Fig. 6c,d shows the HRTEM image and the related FFT pattern of TiO_2 mesocages after rate performance at full charge state, the whole particle was not well crystalline as before, which is in agreement with the Raman results. In spite of a relatively low crystallinity of the anatase TiO_2 mesocages, the lattice fringe of 0.21 nm could be clearly observed from the crystalline area, indicating a slight increase in the d-spacing distance during the repetition of Na^+ insertion and extraction. It's worth mentioning that the tiny nanoparticle subunits in TiO_2 mesocages still keep oriented along the [100] direction after Na^+ insertion and extraction. This result is different from the reports of Kim *et al.*, which demonstrated reversible variation of the lattice of anatase TiO_2 nanorods even after 100 cycles[25]. It's suggested that Na^+ insertion into anatase single crystals is not easy, and a low crystallinity as well as an increase in lattice may provide a lower energy barrier for Na^+ insertion. Herein, the anatase mesocages composed of highly oriented tiny nanocrystal subunits with large surface area and porous nature of mesocages could provide more active reaction sites for Na^+ storage and a good freedom for volume change during Na^+ insertion.

Discussion

Iso-oriented TiO_2 mesocages with mesoporous nature and tunable microstructures were successfully fabricated via a facile synthesis route. The TiO_2 mesocages were used for the first time as anode materials in rechargeable Na-ion batteries, demonstrating a large reversible charge-discharge capacity, good rate capability and cycling performance. This could be attributed to the intrinsic characteristics of the mesocages constructed by crystallographically oriented nanoparticle subunits with few grain boundaries

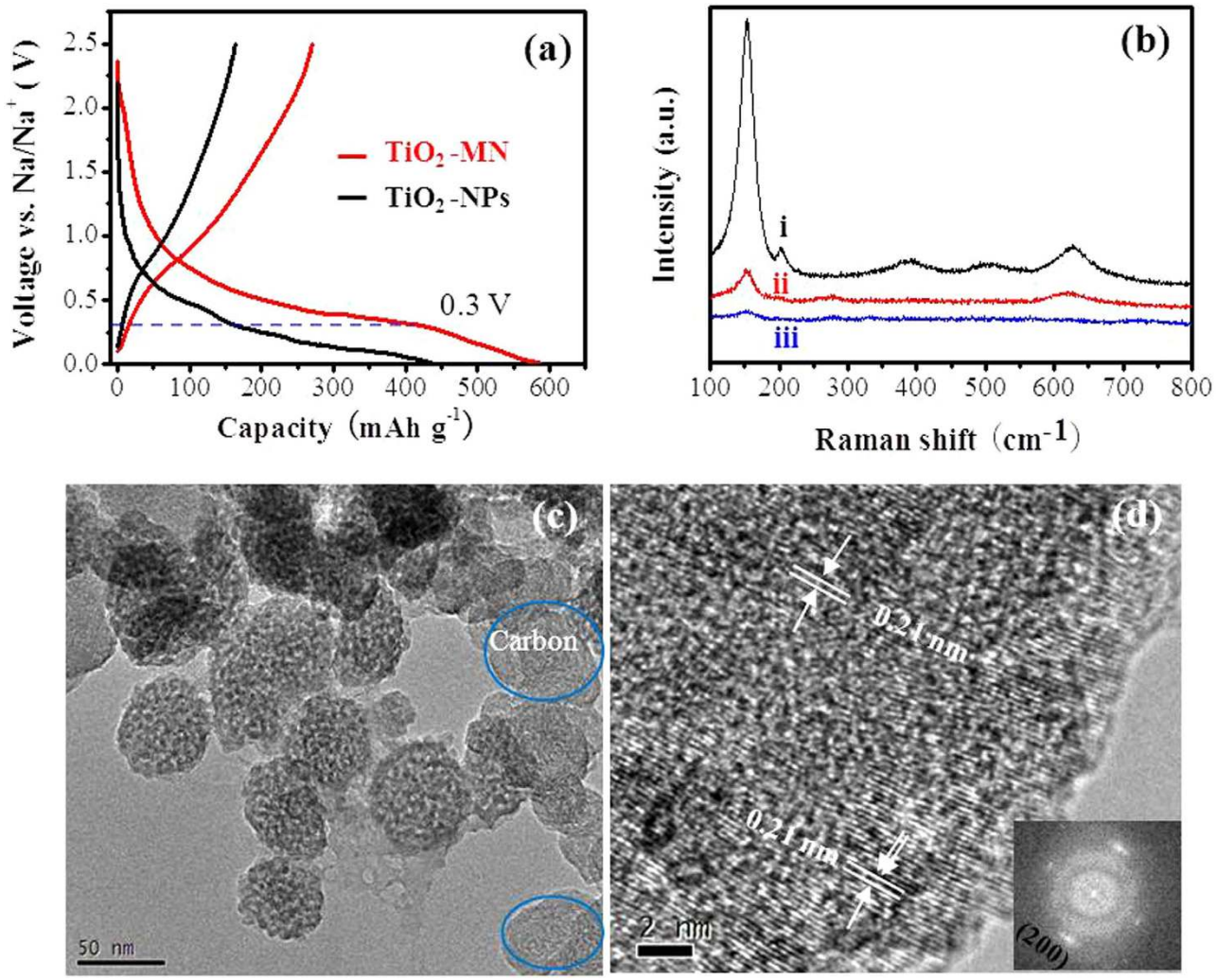

Figure 6. (**a**) The first charge-discharge profiles of TiO_2-MN and TiO_2-NPs, (**b**) Raman spectra obtained from TiO_2-MN electrode at various states: i) fresh, ii) first discharge and iii) first charge, (**c**, **d**) TEM and HRTEM images of TiO_2 mesocages electrode after rate performance. The inset in (**d**) is the related FFT pattern.

compared with the irregularly oriented nanoparticles, accompanied by a large surface area and uniform nanoporous nature. Such architecture facilitated fast electron and ion transport, and gave more active sites and freedom for volume change for Na-ion insertion. Moreover, the sodium-ion storage process of anatase mesocages was mainly controlled by pseudocapacitive behavior, leading to high rate performance and making them promising for applications in rechargeable Na-ion batteries.

Methods

Materials Synthesis. All chemicals were purchased from Aladdin without further purification. In a typical synthesis, 1.5 g sodium dodecyl sulfate (SDS) was first dissolved in 50 mL 2 M HNO_3 or HCl solution. After the solution was stirred for a few minutes, 1 mL (1.5 mL for HCl solution) of titanium (IV) isopropoxide (TIP) was added and kept at 70 °C (80 °C for HCl solution) for 48 h under stirring. The final products were obtained by centrifugation, washed thoroughly with distilled water and dried at 60 °C overnight, and then calcined at 400 °C for 30 min in air to remove the residual organics. The samples obtained from HNO_3 and HCl solution were denoted as TiO_2-MN- and TiO_2-MC, respectively.

Characterizations of the samples. Scanning electron microscopy (SEM, S8010 instrument) and Transmission electron microscopy (TEM, FEI F20 S-TWIN instrument) were applied for the structural characterization of the resulting nanowires and mesocrystals. X-ray diffraction (XRD) patterns were recorded on a Rigaku X-ray diffractometer using Cu Kα ($\lambda = 1.5418$ Å) radiation. N_2 adsorption-desorption analysis was measured on a Micro-meritics TriStar II 3020 instrument (USA). The pore size distributions of the as-prepared samples were analyzed using the Non-Local-Density Functional

Theory (NLDFT) methods. The Raman spectra were recorded on a LabRAM HR Evolution (HORIBA Jobin Yvon) with a 532 nm laser.

Electrochemical Measurements. For the electrochemical measurement of Na-ion intercalation, TiO_2 mesocages were admixed with polyvinylidene fluoride (PVDF) binder and acetylene black carbon additive in a weight ratio of 70:20:10. The mixture was spread and pressed on copper foil circular flakes as working electrodes (WE), and dried at 120 °C in vacuum for 12 h. Na-ion cells were assembled in coin-type cells (CR 2025) with a Na metal foil as the negative electrode, glass fiber separator (Whatman GF/F), and 1 M $NaClO_4$ in ethylene carbonate (EC) and diethyl carbonate (DEC) (1/1 in volume) as the electrolyte. The cells were assembled in a glove box filled with highly pure argon gas (O_2 and H_2O levels < 1 ppm), and charge/discharge tests were performed in the voltage range of 0.01 to 2.5 V (Na^+/Na) on a Land automatic batteries tester (Land CT 2001A, Wuhan, China). The active material content in the electrode was around 1.2 mg cm^{-2}, and the amount of electrolyte was 170–200 μL. The cells were tested under a constant temperature (25 °C). Cyclic voltammetry (CV) measurements were performed on Zennium (Zahner).

References

1. Armand, M. & Tarascon, J. M. Building better batteries. *Nature* **451,** 652–657 (2008).
2. Tarascon, J.-M. Is lithium the new gold? *Nat. Chem.* **2,** 510–510 (2010).
3. Yabuuchi, N., Kubota, K., Dahbi, M. & Komaba, S. Research development on sodium-ion batteries. *Chem. Rev.* **114,** 11636–11682 (2014).
4. Kim, Y., Ha, K.-H., Oh, S. M. & Lee, K. T. High-capacity anode materials for sodium-ion batteries. *Chem. Eur. J.* **20,** 11980–11992 (2014).
5. Pan, H., Hu, Y.-S. & Chen, L. Room-temperature stationary sodium-ion batteries for large-scale electric energy storage. *Energy Environ. Sci.* **6,** 2338–2360 (2013).
6. Stevens, D. A. & Dahn, J. R. The mechanisms of lithium and sodium insertion in carbon materials. *J. Electrochem. Soc.* **148,** A803–A811 (2001).
7. Ge, P. Fouletier. Electrochemical intercalation of sodium in graphite. *Solid State Ion.* **28-30,** 1172–1175(1988).
8. Jache, B. & Adelhelm, P. Use of graphite as a highly reversible electrode with wuperior cycle life for sodium-ion batteries by making use of co-Intercalation phenomena. *Angew.Chem. Int. Ed.* **53,** 10169–10173 (2014).
9. Tang, K. *et al.* Hollow carbon nanospheres with superior rate capability for sodium-based batteries. *Adv. Energy Mater.* **2,** 873–877 (2012).
10. Ponrouch, A., Goñi, A. R. & Palacín, M. R. High capacity hard carbon anodes for sodium ion batteries in additive free electrolyte. *Electrochem. Commun.* **27,** 85–88 (2013).
11. Liu, Y. *et al.* Tin-coated viral nanoforests as sodium-ion battery anodes. *ACS Nano* **7,** 3627–3634 (2013).
12. Xu, Y., Zhu, Y., Liu, Y. & Wang, C. Electrochemical performance of porous carbon/tin composite anodes for sodium-Ion and lithium-ion batteries. *Adv. Energy Mater.* **3,** 128–133 (2013).
13. Wang, L. *et al.* Porous CuO nanowires as the anode of rechargeable Na-ion batteries. *Nano Res.* **7,** 199–208 (2014).
14. Zhu, C., Mu, X., van Aken, P. A., Yu, Y. & Maier, J. Single-layered ultrasmall nanoplates of MoS_2 embedded in carbon nanofibers with excellent electrochemical performance for lithium and sodium storage. *Angew.Chem. Int. Ed.* **53,** 2152–2156 (2014).
15. Senguttuvan, P., Rousse, G., Seznec, V., Tarascon, J.-M. & Palacín, M. R. $Na_2Ti_3O_7$: Lowest voltage ever reported oxide insertion electrode for sodium ion batteries. *Chem. Mater.* **23,** 4109–4111(2011).
16. Pan, H. *et al.* Sodium storage and transport properties in layered $Na_2Ti_3O_7$ for room-temperature sodium-ion batteries. *Adv. Energy Mater.* **3,** 1186–1194 (2013).
17. Zhu, G.-N., Wang, Y.-G. & Xia, Y.-Y. Ti-based compounds as anode materials for Li-ion batteries. *Energy Environ. Sci.* **5,** 6652–6667 (2012).
18. Hong, Z., Wei, M., Lan, T., Jiang, L. & Cao, G. Additive-free synthesis of unique TiO_2 mesocrystals with enhanced lithium-ion intercalation properties. *Energy Environ. Sci.* **5,** 5408–5413 (2012).
19. Hong, Z. & Wei, M. Layered titanate nanostructures and their derivatives as negative electrode materials for lithium-ion batteries. *J. Mater, Chem. A* **1,** 4403–4414 (2013).
20. Ren, H. *et al.* Multishelled TiO_2 hollow microspheres as anodes with superior reversible capacity for lithium ion batteries. *Nano Lett.* **14,** 6679–6684 (2014).
21. Xiong, H., Slater, M. D., Balasubramanian, M., Johnson, C. S. & Rajh, T. Amorphous TiO_2 nanotube anode for rechargeable sodium ion batteries. *J. Phys. Chem. Lett.* **2,** 2560–2565 (2011).
22. Xu, Y. *et al.* Nanocrystalline anatase TiO_2: a new anode material for rechargeable sodium ion batteries. *Chem. Commun.* **49,** 8973–8975(2013).
23. Qin, G., Zhang, X. & Wang, C. Design of nitrogen doped graphene grafted TiO_2 hollow nanostructures with enhanced sodium storage performance. *J. Mater, Chem. A* **2,** 12449–12458 (2014).
24. Cha, H. A., Jeong, H. M. & Kang, J. K. Nitrogen-doped open pore channeled graphene facilitating electrochemical performance of TiO_2 nanoparticles as an anode material for sodium ion batteries. *J. Mater, Chem. A* **2,** 5182–5186 (2014).
25. Kim, K.-T. *et al.* Anatase titania nanorods as an intercalation anode material for rechargeable sodium batteries. *Nano Lett.* **14,** 416–422 (2014).
26. Wu, L. *et al.* Unfolding the mechanism of sodium insertion in anatase TiO_2 nanoparticles. *Adv. Energy Mater.* **2015,** doi: 10.1002/aenm.201401142.
27. Bian, Z. *et al.* Single-crystal-like titania mesocages. *Angew. Chem. Int. Ed.* **123,** 1137–1140 (2011).
28. Song, R. Q. & Cölfen, H. Mesocrystals: Ordered nanoparticle superstructures. *Adv. Mater.* **22,** 1301–1330 (2010).
29. Uchaker, E. & Cao, G. Mesocrystals as electrode materials for lithium-ion batteries. *Nano Today* **9,** 499–524 (2014).
30. Penn, R. L. & Banfield, J. F. Imperfect oriented attachment: Dislocation generation in defect-free nanocrystals. *Science* **281,** 969–971 (1998).
31. Stroppa, D. G. *et al.* Anomalous oriented attachment growth behavior on SnO_2 nanocrystals. *Chem. Commun.* **47,** 3117–3119 (2011).
32. Yin, J., Qi, L. & Wang, H. Sodium titanate nanotubes as negative electrode materials for sodium-ion capacitors. *ACS Appl. Mater. Interfaces* **4,** 2762–2768 (2012).
33. Wang, W. *et al.* Single crystalline $Na_2Ti_3O_7$ rods as an anode material for sodium-ion batteries. *RSC Advances* **3,** 1041–1044 (2013).

34. Brezesinski, T., Wang, J., Tolbert, S. H. & Dunn, B. Ordered mesoporous α-MoO_3 with iso-oriented nanocrystalline walls for thin-film pseudocapacitors. *Nat. Mater.* **9,** 146–151 (2010).
35. Gonzalez, J. R. *et al.* Microstructure of the epitaxial film of anatase nanotubes obtained at high voltage and the mechanism of its electrochemical reaction with sodium. *CrystEngComm* **16,** 4602–4609 (2014).
36. Giarola, M. *et al.* Vibrational dynamics of anatase TiO_2: Polarized Raman spectroscopy and *ab initio* calculations. *Phys. Rev. B* **81,** 174305 (2010).

Acknowledgements

This work was financially supported by National Natural Science Foundation of China (NSFC 21173049 and J1103303), Research Fund for the Doctoral Program of Higher Education of China (RFDP 20133514110002), the Fujian Province Fund (2015J01042, JA14081) and Key Laboratory of Novel Thin Film Solar Cells, CAS.

Author Contributions

Z.S.H. and M.D.W. proposed and designed the experiments. Z.S.H. and K.Q.Z carried out the synthetic experiments and conducted the characterization. Z.S.H. performed the HRTEM, SEM characterization and structural analysis. Z.S.H. and Z.G.H. analysed the data of electrochemical tests. Z.S.H. and M.D.W. wrote the manuscript. All the authors participated in discussions of the research.

Additional Information

Supplementary information accompanies this paper at http://www.nature.com/srep

Competing financial interests: The authors declare no competing financial interests.

How to cite this article: Hong, Z. *et al.* Iso-Oriented Anatase TiO_2 Mesocages as a High Performance Anode Material for Sodium-Ion Storage. *Sci. Rep.* **5**, 11960; doi: 10.1038/srep11960 (2015).